Ratiometric Pulsed Alkylation Mass Spectrometry as a Probe of Thiolate Reactivity in Different Metalloderivatives of *Staphylococcus aureus* pI258 CadC[†,‡]

Julius L. Apuy,[||,§] Laura S. Busenlehner,[⊥,||] David H. Russell,[§] and David P. Giedroc*[,||]

Department of Biochemistry and Biophysics and Department of Chemistry, Center for Advanced Biomolecular Research, Texas A&M University, College Station, Texas 77843-2128

Received September 15, 2003; Revised Manuscript Received January 12, 2004

ABSTRACT: The coordination structure and reactivities of metal ligands in metal-sensing metalloregulatory coordination complexes may well dictate their biological properties. Here, we use the technique of ratiometric pulsed alkylation mass spectrometry (rPA-MS) to probe the structure and reactivities of metal coordination complexes formed by different metalloderivatives of *Staphylococcus aureas* plasmid pI258-encoded CadC, the metal-regulated transcriptional repressor of the *cad* operon. The *cad* operon provides resistance to large thiophilic heavy metal pollutants including Cd(II), Pb(II), and Bi(III). Two cysteines, an invariant Cys7 and a conserved Cys11, separated by three amino acids near the N-terminus of each subunit within dimeric CadC, donate two of the four coordination bonds to Cd(II) and Bi(III); in contrast, Cys11, but not Cys7, is excluded from the trigonal Pb(II) complex. rPA-MS reveals that Cys7 is strongly protected from alkylation in all metal complexes, Pb(II) being most effective, reducing k_{C7}^{app} by ∼1000-fold relative to apo-CadC; in contrast, the reactivity of Cys11 is indistinguishable from that of apo-CadC, consistent with an S_3 coordination complex. Only in the tetrathiolate complexes formed by Cd(II) and Bi(III) is the reactivity of Cys11 appreciably reduced, but only by ≥10-fold. These data suggest that the Cys11-S^-−metal coordination bond or that side of the coordination chelate in the trigonal Pb(II) complex defines a "weak point" in the chelate and thus might provide an entry site for potential metal ligand exchange reactions important for metal resistance in vivo. In contrast, Cys7 forms a tight coordination bond with all inducing metals, consistent with its role as a critical allosteric ligand in the metalloregulation of the operator/promoter binding.

Many bacteria have evolved resistance to high concentrations of both biologically required and toxic heavy metal pollutants that might be encountered in their environments (*1*−*4*). Plasmid- or chromosomally encoded resistance genes are usually grouped together in an operon of which the expression is tightly controlled by a transcriptional regulatory protein that specifically "senses" toxic metal ions (*5*). *Staphylococcus aureus* plasmid pI258-encoded CadC is a metalloregulatory transcriptional repressor (*6*) from the SmtB/ArsR family (*7*, *8*) that controls the transcription of the *cad* operon. The *cad* operon confers resistance to heavy metal ions such as Cd(II), Pb(II), Zn(II), and Bi(III) (*9*). In response to an increase in the intracellular concentrations of these metal ions, the CadC repressor, which specifically binds to the *cad* operator/promoter (O/P) (*6*, *10*), coordinates metal ions and transcription from the *cad* O/P is de-repressed. This allows for expression of both CadA, an integral membrane metal efflux protein that specifically transports Pb(II), Cd-(II), and Zn(II) out of the cell (*11*), and CadC itself.

Previous work has revealed that CadC is a weakly dissociable, noncovalent homodimer that binds to the *cad* O/P with high affinity ($K_a = 1 \times 10^9$ M^{-1}; 0.4 M NaCl, pH 7.0) (*10*). Direct binding of inducing metal ions results in a significant decrease in the affinity of the protein for the operator/promoter ($K_a \approx 10^6$ M^{-1}), consistent with a simple model of metal-mediated dissociation as the mechanism of induction of the *cad* operon (*10*, *12*, *13*). CadC is therefore a metalloregulated transcriptional repressor that senses toxic, thiophilic metals. It is currently unknown how CadC-bound metal ions then migrate to the actual sites of resistance, for example, to CadA; however, efficient metal ligand exchange with an acceptor small molecule or resistance protein itself may well be involved (*14*, *15*).

S. aureus pI258 CadC contains five cysteines per monomer located at amino acid residue positions 7, 11, 52, 58, and 60. Cys7 and Cys11 are located near the N-terminus of the protein, while homology modeling with the related zinc sensor, *Synechococcus* SmtB (*16*), makes the prediction that Cys58 and Cys60 are found in the α3 helix of the conserved

[†] This work was supported by grants from the National Institutes of Health (Grant GM042569) and the Robert F. Welch Foundation (Grant A-1275) to D.P.G. and the U.S. Department of Energy, Division of Chemical Sciences, BES (Grant DE-FG03-95ER14505), and the National Science Foundation (Grants CHE-9629966 and DBI-0116685) to D.H.R.

[‡] This work was submitted by J.L.A. in partial fulfillment of the requirements for a Ph.D. in Chemistry at Texas A&M University.

* To whom correspondence should be addressed. E-mail: giedroc@tamu.edu; Tel: 979-845-4231; Fax: 979-845-4946.

[||] Department of Biochemistry and Biophysics.

[§] Department of Chemistry.

[⊥] Present address: Department of Biochemistry and the Center for Molecular Toxicology, Vanderbilt University School of Medicine, Nashville, TN 37232-0146.

10.1021/bi035668f CCC: $27.50
Published on Web 03/03/2004

^{56}EL**C**V**C**^{61}D motif as part of the proposed α3-T-α4 helix-turn-helix DNA binding domain (*12*). Cys7, Cys58, and Cys60 are invariant, and Cys11 is moderately conserved, while Cys52 is not conserved among all functionally identified CadC proteins (*8*, *17*). Previous spectroscopic studies with wild-type and single cysteine-substitution mutants of CadC have revealed that cysteines 7, 11, 58, and 60 constitute the metalloregulatory tetrathiolate α3N metal binding site for Cd(II) and Bi(III); Co(II) and Zn(II) are thought to form the same highly distorted S_4 tetrathiolate metal complex (*13*). In contrast, the first coordination sphere of Pb(II) is composed of only the three invariant cysteines 7, 58, and 60 with cysteine 11 not donating a coordination bond to the Pb(II) ion (*13*). Cd(II) X-ray absorption spectroscopy (XAS) of CadC is also consistent with a tetrahedral S_4 Cd(II) center with an average Cd−S bond length of 2.53 Å (*10*), while Pb(II) XAS of CadC was most consistent with a trigonal S_3 complex with an average Pb−S bond length of 2.66 Å (*13*). These studies reveal that the thiolate-rich α3N site is capable of forming at least two distinct coordination complexes and is capable of altering its coordination geometry to accommodate the binding of distinct metal ions.

We have recently developed a sensitive analytical method, termed ratiometric pulsed alkylation mass spectrometry (rPA-MS) (*18*, *19*), that measures the apparent second-order rates of reactivities of cysteine thiolates toward the sulfhydryl-specific alkylating reagent *N*-ethylmaleimide (NEM) (*19*). The method is ratiometric along a reaction coordinate, where cysteine residues are subjected to modification with deuterated d_5-NEM for some pulse time, *t*, and chased with a large excess of light NEM, H_5 (or d_0)-NEM (*19*); cysteine reactivities are directly encoded in the ratio of d_5-NEM- vs H_5-NEM-derivatized cysteine-containing peptides resolved on a mass spectrometer. This approach has parallels to the misincorporation proton-alkyl exchange (MPAX) technique, used to monitor solvent accessibility of cysteines (*20*), and to global internal standard strategies used in quantitative protein expression profiling in proteomics applications, which like rPA-MS also make use of isotope coding of alkylating and acylating reagents (*21*−*23*). The application of rPA-MS to the cysteine thiolate pairs in individual Cys_2His_2 zinc finger domains in the human metalloregulatory protein, MTF-1,[1] revealed that individual zinc finger coordination chelates are characterized by distinct stabilities, kinetic labilities, or both thus providing insight into the functional heterogeneity of zinc fingers in this metalloregulatory protein (*19*). Here, this method has been used to obtain residue-specific insight into the reactivity of coordinating thiol(ate) ligands in a single metal complex and the extent to which the reactivity of each is attenuated by the binding of different metal ions to apo-CadC. We find that the critical allosteric ligand Cys7 and the partially conserved Cys11 vary dramatically in their relative reactivities toward NEM in a manner that depends on the nature of the metal ion. The structural and functional implications of these findings are discussed.

[1] Abbreviations: DTNB, 5,5′-dithiobis(2-nitrobenzoic acid); MTF-1, metal-response element (MRE)-binding transcription factor-1; d_5-NEM, d_5-*N*-ethylmaleimide; H_5-NEM, *N*-ethylmaleimide; MALDI-TOF, matrix-assisted laser desorption ionization time-of-flight; O/P, operator/promoter.

MATERIALS AND METHODS

Materials. 2-(*N*-Morpholino)ethanesulfonic acid (MES), [bis(2-hydroxyethyl)amino]tris(hydroxymethyl)methane (Bis-Tris), bradykinin, and 5,5′-dithiobis(2-nitrobenzoic acid) (DTNB)[1] were from Sigma. Dithiothreitol was obtained from Acros-Organics, and Chelex-100 resin was purchased from Bio-Rad. d_5-NEM[1] (*N*-ethylmaleimide) was obtained from Medical Isotopes, Inc., while H_5-NEM[1] was purchased from ICN. d_5-NEM differs from H_5-NEM in that all five hydrogen atoms of the *N*-ethyl substituent are substituted with deuterium. Trifluoroacetic acid was obtained from Pierce Chemicals and HPLC-grade acetonitrile was purchased from EM Science Corp. Sequencing-grade trypsin was supplied by Promega, while chymotrypsin was purchased from Boehringer-Mannheim. Ultrapure cadmium(II) chloride, bismuth(III) nitrate, lead(II) chloride, zinc(II) sulfate, and cobalt(II) chloride were purchased from Johnson Matthey.

Expression and Purification of CadC. Wild-type CadC was overexpressed from the pET-CadC plasmid construct in *Escherichia coli* strain BL21(DE3)/pLysS and purified as previously described (*10*). The concentration of the purified "metal-free" CadC was determined using the calculated molar extinction coefficient of 6585 M^{-1} cm^{-1} at 280 nm (*10*). "Metal-free" CadC contained less than 0.03 mol of Zn(II) per CadC monomer as determined from Zn(II) atomic absorption spectroscopy as described (*10*). The number of free cysteine thiols per CadC monomer was calculated using a standard DTNB[1] assay in an anaerobic glovebox. Wild-type CadC was found to contain 3.8 ± 0.2 free thiols per monomer out of 5 possible free cysteine thiols. Typical metal/protein monomer stoichiometries reached at saturation were 0.8:1 (*13*), consistent with the partial inactivation of some metal binding sites due to an intersubunit disulfide bond between Cys58 and either Cys7 or Cys11 in the N-terminal region (*12*).

Ratiometric Pulsed Alkylation. Apo-, Cd(II)-, Zn(II)-, and Co(II)-CadC samples were prepared in MES buffer (5 mM MES, 0.40 M NaCl, pH 7.0), while the Pb(II)- and Bi(III)-CadC complexes were prepared in a weakly chelating Bis-Tris buffer (5 mM Bis-Tris, 0.40 M NaCl, pH 7.0). Cd(II), Pb(II), and Bi(III) were added to apo-CadC to yield a 1:1 molar ratio of metal ion to CadC monomer, referred to as apo-, Cd_1-, Pb_1-, and Bi_1-CadC. For the preparation of Zn(II)- and Co(II)-substituted CadCs, metals were added to apo-CadC in a 2:1 metal/CadC monomer ratio to fill both thiolate-rich α3N and N/O-containing α5 sites (referred to as Zn_2- and Co_2-CadCs) (*13*). These solutions were diluted with the appropriate buffer to obtain 2 mL samples of 8.56 μM apo- or metalated-CadC for the pulsed alkylation experiments.

Pulsed alkylation was carried out in a Vacuum-Atmospheres anaerobic (≤0.7 ppm O_2) glovebox at ambient temperature (~25 °C). The 8.56 μM CadC samples (apo-, Cd_1-, Pb_1-, Bi_1-, Zn_2-, and Co_2-; 33 μM total reduced Cys) were individually pulsed alkylated with the addition of d_5-NEM to a final concentration of 528 μM (16-fold molar excess over reduced cysteine residues). At different pulsed time intervals, a 200 μL aliquot of pulsed alkylated protein was removed and added to H_5-NEM to a final concentration of 9.7 mM (290-fold molar excess over reduced cysteine residues). Approximately half of this sample was removed and added to 0.13 μg/μL chymotrypsin with the remaining

Table 1: Amino Acid Sequences and Masses of Unmodified and NEM-Alkylated Chymotryptic (C) and Tryptic (T) Peptides of *S. aureus* pI258 CadC Identified in This Study

				mass of NEM-derivatized peptides (Da)			
				H_5		d_5	
peptide	Cys residue	amino acid sequence	mass (Da)	calcd	obsd	calcd	obsd
C^{1-10}	Cys7	[1]MKKKDT**C**EIF	1242.62	1367.66	1367.64	1372.46	1372.44

				mass of NEM-derivatized peptides (Da)					
				H_5,H_5		H_5,d_5		d_5,d_5	
peptide	Cys residue	amino acid sequence	mass (Da)	calcd	obsd	calcd	obsd	calcd	obsd
T^{5-16}	Cys7/Cys11	[5]DT**C**EIF**C**YDEEK	1494.58	1744.67	1744.65	1749.23	1749.19	1754.26	1754.22

half added to 0.1 μg/μL trypsin. The proteolysis reactions were allowed to proceed overnight at ambient temperature then subsequently removed from the glovebox and prepared for elution from a C4 microtip column (Amika Corporation). The tip columns were first washed with HPLC-grade acetonitrile before equilibration with 0.1% trifluoroacetic acid (TFA). The digested samples were individually loaded onto the C4 column, washed with 0.1% TFA, then eluted with 0.1% TFA in 100% acetonitrile. The samples were vacuum-centrifuged to dryness and resuspended in 30 μL of deionized, distilled water. An aliquot of each sample was then diluted to a final protein concentration of ~0.1 mg/mL in a solution containing 1.5 mg/mL ferulic acid in 25% aqueous methanol. These samples were then deposited as a series of 500 nL spots on top of an air-dried layer of matrix made by spotting 5 μL of a 30 mg/mL solution of α-cyano-4-hydroxycinnamic acid in pure methanol.

MALDI-TOF Mass Spectrometry. MALDI-TOF[1] mass spectra of all samples were acquired using a Perseptive Biosystem Voyager Elite XL TOF mass spectrometer equipped with a pulsed nitrogen laser emitting at 337 nm manufactured by Laser Science Inc. All spectra were acquired in the positive ion mode using 25 kV acceleration with each spectrum representing the average of 100 laser pulses. The spectra for the tryptic and chymotryptic peptide fragments of apo- and metalated-CadC were acquired with a 200 ns delayed extraction (DE) time in the reflectron mode. The grid and the guide wire voltages were operated at 70% and 0.05% of the acceleration voltage, respectively. Bradykinin $[1060.5\ Da]^{1+}$ was used as external calibration of the mass spectrometer. The mass resolution, expressed as $M/\Delta M$, from these experiments was ~15 000, and measurement accuracy was typically 10−15 ppm with a reproducibility between samples of ±0.2 ppm.

Ratiometric Quantitation of Isotopically Differentiated Mass Peaks. Two different MALDI-TOF mass spectra were acquired for each d_5-NEM time pulse/H_5-NEM chase experiment and processed using GRAMS/32 (Galactic Industries Inc.) for peak localization and integration. Integration was over the sum of the peak areas of the full isotopic distribution. One mass spectrum contains a complete set of chymotryptic peptides of CadC, in which the peptide containing Cys7 (C^{1-10}) is fully alkylated by NEM and resolved either as an H_5-NEM-derivatized peptide (mass = expected peptide mass + 125 mu) or as a d_5-NEM-derivatized peptide (mass = expected peptide mass + 130 mu) (see Table 1). The second mass spectrum contains a complete set of tryptic peptides of CadC, including the peptide denoted T^{5-16}, in which both Cys7 and Cys11 are alkylated by NEM and resolved as either an H_5,H_5-NEM-derivatized peptide (mass = expected peptide mass + 250 mu), an H_5,d_5-NEM-derivatized peptide (mass = expected peptide mass + 255 mu), or a d_5,d_5-NEM-derivatized peptide (mass = expected peptide mass + 260 mu) (Table 1).

The mole fraction (Θ) of each of the two singly derivatized (d_5 and H_5) peptides in a mixture is calculated as the ratio of the peak area integration (A) of the ith NEM-derivatized species to the sum of the integrated areas of all ($H_5 + d_5$) alkylated species. For example, the mole fraction of the d_5-derivatized C^{1-10} peptide, $\Theta(d_5)$, is defined as

$$\Theta(d_5) = A(d_5)/[A(H_5) + A(d_5)]$$

and correspondingly, the mole fraction (Θ) of the d_5,d_5-NEM doubly derivatized T^{5-16} peptide containing Cys7 and Cys11 is defined as

$$\Theta(d_5,d_5) = A(d_5,d_5)/[A(H_5,H_5) + A(H_5,d_5) + A(d_5,d_5)]$$

As the pulse time of the d_5-NEM reactivity increases, Θ-(d_5) and $\Theta(d_5,d_5)$ will increase with other species correspondingly decreasing, since any cysteine thiolate that survives the d_5-NEM pulse is subsequently alkylated in the chase by an NEM solution containing ~18:1 molar ratio of H_5-NEM to d_5-NEM. A chase designed in this way should derivatize all unmodified cysteine-containing peptides that survive the d_5-NEM pulse; this was verified for Cys7 and Cys11 by comparing the full MALDI-TOF spectra of trypsin-digested underivatized CadC with that of CadC derivatized with H_5-NEM according to these chase conditions (data not shown).

Calculation of the Apparent Second-Order Rates of the Reactive Thiolates. The apparent rate of reactivity of Cys7 toward d_5-NEM was determined by fitting the ratiometric data obtained for the chymotryptic C^{1-10} peptide to a sum of two exponentials or by fitting it to a unimolecular irreversible reaction mechanism (Y → Z; k_1) using the Berkeley Madonna curve fitting program. The double-exponential function is

$$\Theta_{H_5} = 1 - \Theta_{d_5} = [A_{i,0} \exp^{-(k_f t)} + (1 - A_{2,0}) \exp^{-(k_s t)}]$$

where t = time (min), k_f = fast rate, k_s = slow rate, and $A_{i,0}$ = mole fraction at $t = 0$. The double-exponential function was required to account for the presence of a small fraction (~14−25%) of fast reacting thiolates in all preparations of metalated-CadCs, due to inactivation of some metal binding sites by partial cysteine oxidation (*10*, *12*).

The apparent rate of reactivity of Cys11 was determined by fitting the time-dependent ratiometric data acquired for T^{5-16} to a unimolecular two-step reaction model: X → Y → Z (X → Y, k_1, and Y → Z, k_2). The mole fraction of reaction species X was assigned to $\Theta(H_5,H_5)$, Y to $\Theta(H_5,d_5)$, and Z to $\Theta(d_5,d_5)$ derived from the ratiometric data for T^{5-16}. The individual k_i^{app} were converted to apparent second-order rates for Cys7 and Cys11 by dividing the k_i resolved from curve-fitting by 5.28×10^{-4} M d_5-NEM. For Bi(III)-CadC, the ratiometric data were also fit to a branched pathway in which X→ Y → Z or X → Z with the apparent rate for the X → Z reaction defined as k_3.

RESULTS

Identification of Proteolytic Peptides of CadC. Complete proteolytic digests (trypsin and chymotrypsin) of CadC were subjected to mass analysis using high-resolution MALDI-TOF mass spectrometry. Mass spectral analysis of the tryptic digest of apo-CadC led to the identification of a peak with a *m*/*z* of 1494.58, which is assigned to peptide that contains Cys7 and Cys11, denoted T^{5-16} (expected $m/z = 1494.67$; Table 1). In addition, the mass spectrum of the chymotryptic digest of CadC contains a peak with a *m*/*z* of 1242.62 that is consistent with a peptide that contains only Cys7, denoted C^{1-10} (Table 1). To confirm the identity of these peptides, complete MALDI-TOF spectra were obtained for digests of CadC subjected to complete alkylation of reactive cysteines by *N*-ethylmaleimide (NEM) under the chase conditions described (see Materials and Methods). As expected, NEM alkylation results in a quantitative mass shift of peptide C^{1-10} by 125 mu due to derivitization of Cys7 and of peptide T^{5-16} by 250 mu as a result of alkylation of both Cys7 and Cys11 (Table 1). Ratiometric mass data for the remaining cysteines in CadC, Cys52, Cys58, and Cys60, while theoretically possible, could not be obtained in practice perhaps because of the size (~3500 Da) and complexity of the smallest tryptic peptide containing these three cysteines (*19*).[2]

Reactivities of Cysteine Thiolates at Positions 7 and 11 of Apo-CadC. Briefly, in a ratiometric pulsed alkylation mass spectrometry experiment (*19*), the kinetics of alkylation of cysteine thiolates by the electrophile *N*-ethylmaleimide (NEM) is determined by exposing the protein to a pulse of variable time duration with a large (≥10-fold) excess of perdeuterated d_5-NEM over cysteine thiolates. This pulse is subsequently followed by a chase with ≥100-fold excess protonated H_5-NEM to fully derivatize the cysteine thiolates in the protein. Following complete proteolysis by trypsin or chymotrypsin, the extent of derivatization by d_5- and H_5-NEM at individual cysteine residues as a function of pulse time is determined by high-resolution MALDI-TOF mass spectrometry and peak integration of differentially alkylated peptides.

An expanded view of the region of the chymotryptic MALDI-TOF mass spectrum containing the C^{1-10} peptide of apo-CadC is shown in Figure 1 (upper left). The spectrum

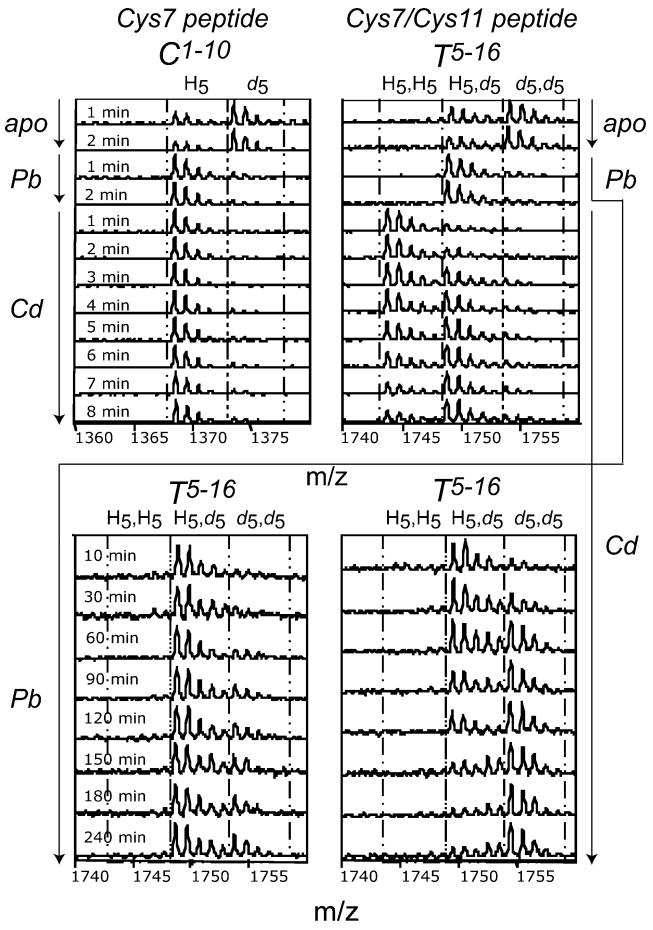

FIGURE 1: A series of MALDI-TOF spectra localized on either the chymotryptic peptide C^{1-10} (upper left panel) or the tryptic peptide T^{5-16} (upper right, lower two panels) recovered from either apo-, Pb(II)-, or Cd(II)-CadC digests as a function of pulse alkylation time with d_5-NEM (pulse times are indicated on the left-most panel and can be read directly across).

shows that the majority of the C^{1-10} peptide containing only Cys7 is modified by d_5-NEM at the initial time points of pulsed alkylation with the full time course (Figure 2A) revealing derivatization of Cys7 is complete within 5 min of d_5-NEM pulse alkylation time. This reveals an apparent pseudo-first-order alkylation rate of Cys7 in apo-CadC of 1.07 min^{-1}, which when divided by the total concentration of d_5-NEM gives an apparent second-order rate constant of 1.93×10^3 M_{NEM}^{-1} min^{-1}. This value is comparable to that obtained for a solvent-exposed cysteine in bacterial luciferase under similar solution conditions (*24*) but slower than Cys_2−His_2 zinc finger thiolates in apo-MTF-1 and apo-Sp1 (*19*).

The early time points of the kinetics of alkylation of T^{5-16} are also shown in Figure 1 (upper right) for apo-CadC. Interestingly, the H_5,H_5-NEM mass peak of the doubly alkylated tryptic peptide T^{5-16} (Cys7 and Cys11) is completely absent at the earliest stages of pulsed alkylation of apo-CadC; furthermore, the mole fractions of H_5,d_5- and d_5,d_5-derivatives of T^{5-16} were found to be identical (data not shown) to the mole fraction of H_5- and d_5-derivatized C^{1-10} peptides, respectively (Figure 2A), revealing that both pairs of mass peaks report on the intrinsic rate of alkylation of Cys7. Since there is no measurable H_5,H_5-derivatization of the T^{5-16} peptide at the initial time points, the apparent rate of reactivity of Cys11 (k_{C11}^{app}) cannot be measured since

[2] It should have been possible to obtain ratiometric mass data on the T^{47-78} peptide that contains Cys52, Cys58, and Cys60 (*12*), even without adjusting the delayed extraction (DE) tuning (*41*). Unfortunately, repeated attempts to acquire these data were unsuccessful, perhaps because of the low yield of fully NEM-derivatized T^{47-78} recovered from tryptic digests.

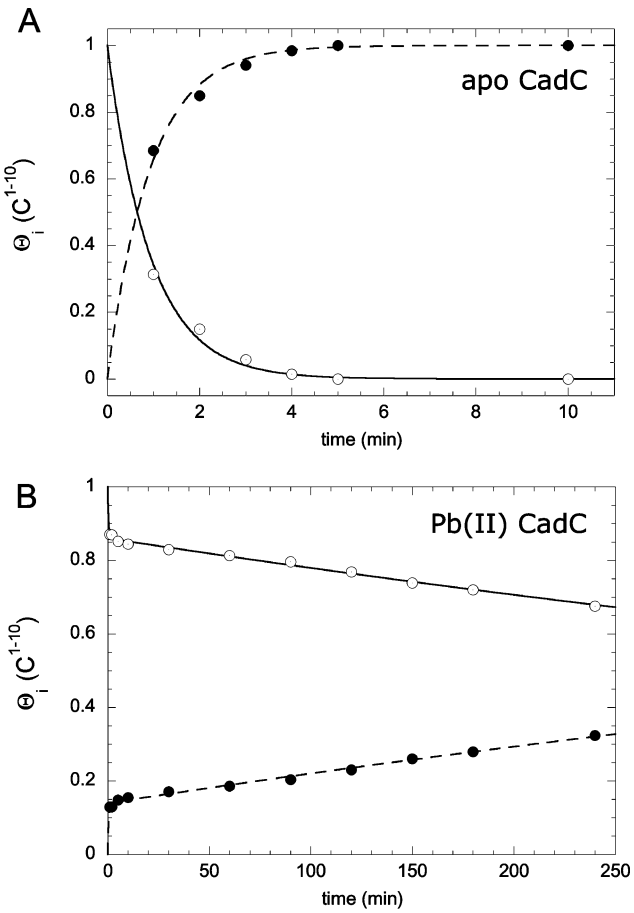

FIGURE 2: rPA-MS of Pb(II)-substituted CadC. Panel A shows the mole fraction of (○) H_5-NEM- and (●) d_5-NEM-derivatized C^{1-10} peptide recovered from apo-CadC rPA-MS chymotryptic digests as a function of d_5-NEM pulse time derived from data like that shown in Figure 1 (upper left panel). The smooth lines are a fit to single irreversible reaction, H_5-NEM-C^{1-10} (Y) → d_5-NEM-C^{1-10} (Z), defined by the rate $k = 1.07 \pm 0.05$ min^{-1}. Panel B shows the mole fraction of (○) H_5-NEM- and (●) d_5-NEM-derivatized C^{1-10} peptide recovered from Pb(II)-CadC rPA-MS chymotryptic digests as a function of d_5-NEM pulse time. The solid line through the experimental data is a least-squares fit to a sum of two exponentials that define a fast phase (characterized by a rate, k_f, and amplitude, A_f) followed by a slow phase (k_s, A_s) (see Materials and Methods). $k_f = 2.36 \pm 0.6$ min^{-1}; $A_f = 0.136$; $k_s = 0.000\,985 \pm 0.000\,036$ min^{-1}; $A_s = 0.864$ (see text for details). An analogous plot of the mole fraction of d_5,H_5- and d_5,d_5-derivatized T^{5-16} peptide recovered from tryptic digests gave similar kinetic parameters (data not shown).

it is fully alkylated prior to the first pulse time measurement (1 min). However, based on the alkylation rate of non-metal-coordinated zinc finger cysteines (*19*), a lower limit is $k^{app} \geq 2.6$ min^{-1} or $\geq 5 \times 10^3$ M_{NEM}^{-1} min^{-1} for Cys11 of apo-CadC.

Reactivities of Cysteine Thiolates at Residue Positions 7 and 11 in Pb(II)-CadC. Investigation of the C^{1-10} mass window for the Pb(II)-derivative of CadC at early pulse times reveals that the Cys7-containing chymotryptic peptide, in contrast to apo-CadC, is primarily in the H_5-modified form (Figure 1, upper left) with the full progress curve shown in Figure 2B. The ratiometric data were fitted to a double-exponential function (see Materials and Methods) characterized by two widely different rates. The fast phase corresponds to a fractional amplitude, A_f, of 0.14 and a rate, k_f, of 2.4 min^{-1} with the slow phase giving $A_s = 0.86$ and $k_s = 9.85 \times 10^{-4}$ min^{-1}. The simplest interpretation of this reaction profile is that the initial fast phase corresponds to alkylation of Cys7 in the small fraction of apo-CadC in Pb(II)-CadC preparations due to inactivation of these metal binding sites by disulfide bond formation (*12*). The slow phase therefore corresponds to alkylation of Cys7 in the Pb(II) coordination complex; therefore, $k_s = k_{C7}^{app}$ $(9.8 \pm 0.3) \times 10^{-4}$ min^{-1}, giving an apparent second-order rate constant of 1.87 M_{NEM}^{-1} min^{-1}. The reactivity of Cys7 is therefore attenuated ~1000-fold upon coordination to Pb(II).

Strikingly, the T^{5-16} mass window for Pb(II)-CadC (Figure 1, upper right to lower left) shows the complete absence of the H_5,H_5-derivatized T^{5-16} mass peak at all d_5-NEM pulse times, analogous to that observed for apo-CadC. However, in contrast to apo-CadC, the majority of the T^{5-16} peptide remains in the H_5,d_5-modified form throughout the time course of the experiment (Figure 1). Since $\Theta_{H5,H5}(T^{5-16})$ is equal to zero at all time points, the mole fractions of H_5- and d_5-derivatized C^{1-10} peptides (Figure 2B) were found to be identical to that of H_5,d_5- and d_5,d_5-derivatized T^{5-16} species, respectively (data not shown).

Reactivities of Cysteine Thiolates at Residue Positions 7 and 11 in Cd(II)-CadC. Like the Pb(II)-derivative, analysis of the C^{1-10} peptides for the Cd(II) complex of CadC indicate mostly all H_5-modified C^{1-10} peptide (Figure 1, upper left) with the integrated mole fraction of H_5-C^{1-10} and d_5-C^{1-10} for the complete time course shown in Figure 3A. As with the Pb(II) complex, the ratiometric data are adequately fit to a sum of two exponentials with the same fractional amplitude and similar rate of reactivity resolved for the fast reacting complex ($A_f = 0.14$; $k_f = 0.67$ min^{-1}); this is consistent with the same concentration of apo-CadC in Cd-(II)-CadC preparations, as expected. Thus, $k_{C7}^{app} = (6.2 \pm 0.3) \times 10^{-3}$ min^{-1}, yielding an apparent second-order rate constant of 11.7 M_{NEM}^{-1} min^{-1}. Cys7 in the Cd(II) coordination complex is about 6-fold more reactive than that in the Pb(II) complex.

In contrast to the mass spectra from tryptic digests of apo and Pb(II)-CadC, the H_5,H_5 mass peak of T^{5-16} constitutes a major fraction among the doubly alkylated species at the early stages of pulsed alkylation in Cd(II)-CadC and is not completely depleted until the 30 min d_5-NEM pulse time (Figures 1 and 3B). Upon depletion of the H_5,H_5-T^{5-16} species, the H_5,d_5-T^{5-16} species is subsequently populated at the early and middle stages of alkylation rate profile (3−30 min), but then is converted to d_5,d_5-T^{5-16} species at longer pulse times (Figures 1 and 3B). Such a reaction profile is fully consistent with a sequential reaction. The continuous lines drawn through the $\Theta_i(T^{5-16})$ data describe a simultaneous nonlinear least-squares fit to a sequential irreversible X → Y → Z reaction model, where $X = \Theta_{H_5,H_5}$, $Y = \Theta_{H_5,d_5}$ and $Z = \Theta_{d_5,d_5}$, described by two rates, k_1 and k_2. Since the rate of conversion of the H_5,d_5-species to the d_5,d_5-species defined by k_2 (6.8×10^{-3} min^{-1}) is comparable to the rate of conversion of H_5-C^{1-10} to d_5-C^{1-10} (compare part A to part B in Figure 3), that is, $k_2 = k_{C7}^{app}$, then k_2 reflects primarily on the apparent rate of alkylation of Cys7. Therefore, k_1^{app} must correspond primarily to the apparent rate of the alkylation of Cys11 in Cd(II)-CadC (k_{C11}^{app}).

Reactivities of Cysteine Thiolates at Residue Positions 7 and 11 in Bi(III)-CadC. The corresponding rPA-MS data

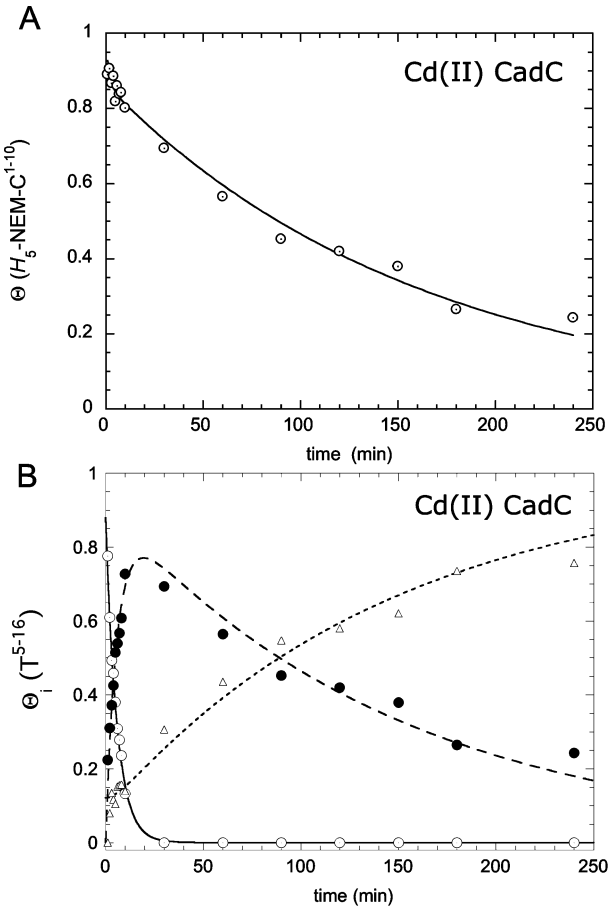

FIGURE 3: rPA-MS of Cd(II)-substituted CadC. Panel A shows the mole fraction of H_5-NEM-derivatized C^{1-10} peptide recovered from Cd(II)-CadC rPA-MS chymotryptic digests as a function of d_5-NEM pulse time. The solid line through the data is a least-squares fit to a sum of two exponentials with $k_f = 0.67 \pm 0.33$ min^{-1}, $A_f = 0.136 \pm 0.016$, $k_s = 0.006\,16 \pm 0.000\,32$ min^{-1}, and $A_s = 0.864$ (see text for details). Panel B shows the mole fraction of (○) H_5,H_5-, (●) H_5,d_5-, and (△) d_5,d_5-NEM-derivatized T^{5-16} peptide recovered from tryptic digests of Cd(II)-CadC as a function of d_5-NEM pulse time. The continuous lines through the data are nonlinear least-squares fits derived from a kinetic model containing two irreversible steps: H_5,H_5-T^{5-16} (X) → H_5,d_5-T^{5-16} (Y) → d_5,d_5-T^{5-16} (Z) in which A_i is the initial amplitude of the ith species, k_1 defines X → Y, and k_2 defines Y → Z. Resolved parameters are $A_X = 0.88$, $A_Y = 0$ (fixed), $A_Z = 0.12$, $k_1 = 0.173$ min^{-1}, and $k_2 = 0.006\,78$ min^{-1}. Note that $A_X \approx A_s$ and $k_2 \approx k_s$ from C^{1-10} digests (panel A) consistent with the fact that both events are monitoring the alkylation rate of Cys7.

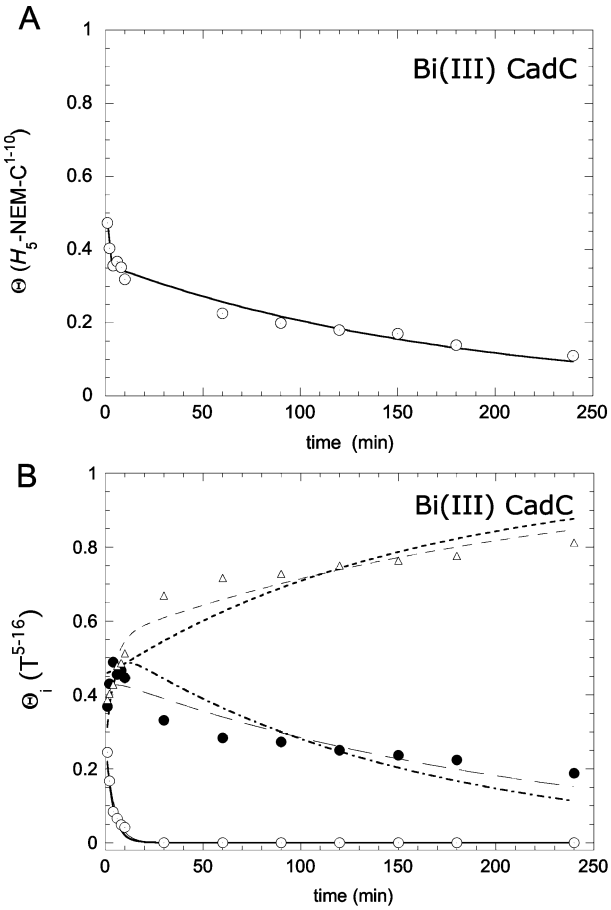

FIGURE 4: rPA-MS of Bi(III)-substituted CadC. Panel A shows the mole fraction of H_5-NEM-derivatized C^{1-10} peptide recovered from Bi(III)-CadC rPA-MS chymotryptic digests as a function of d_5-NEM pulse time. The solid line through the data is a least-squares fit to a sum of two exponentials with $k_f = 1.64 \pm 0.17$ min^{-1}, $A_f = 0.64$, $k_s = 0.005\,60 \pm 0.000\,45$ min^{-1}, and $A_s = 0.36$ (see text for details). Panel B shows the mole fraction of (○) H_5,H_5-, (●) d_5,H_5-, and (△) d_5,d_5-NEM-derivatized T^{5-16} peptide recovered from tryptic digests of Bi(III)-CadC as a function of d_5-NEM pulse time. Two independent fits to the kinetic data are shown: model 1 (cf. Figure 3B), H_5,H_5-T^{5-16} (X) → d_5,H_5-T^{5-16} (Y) → d_5,d_5- T^{5-16} (Z); model 2, H_5,H_5-T^{5-16} (X) → d_5,H_5-T^{5-16} (Y) → d_5,d_5- T^{5-16} (Z) superimposed on H_5,H_5-T^{5-16} (X) → d_5,d_5- T^{5-16} (Z), defined by k_3. Fitted parameters for model 1 (represented by the thick lines) are $A_X = 0.28$, $A_Y = 0.26$, $A_Z = 0.46$, $k_1 = 0.262$ min^{-1}, and $k_2 = 0.006\,52$ min^{-1}. Fitted parameters for model 2 (represented by the thin lines) are $A_X = 0.28$, $A_Y = 0.42$, $A_Z = 0.30$, $k_1 = 0.021$ min^{-1}, $k_2 = 0.0045$ min^{-1}, and $k_3 = 0.20$ min^{-1}. Although neither model fully satisfactorily fits the progress curves, the significant recovery of H_5,H_5-T^{5-16} at early d_5-NEM pulse times qualitatively reveals that Bi(III) protects Cys11 from alkylation, like Cd(II).

acquired for peptides C^{1-10} and T^{5-16} obtained from digests of Bi(III)-CadC (Figure 4) were found to be qualitatively similar to that of Cd(II)-CadC, except that the apparent mole fraction of rapidly reacting Cys7 is much larger, $A_f = 0.64$ and $k_f = 1.64$ min^{-1} (Figure 4A) (see Discussion). k_{C7}^{app} estimated from these data is $(5.6 \pm 0.5) \times 10^{-3}$ min^{-1}, similar to that of Cd(II)-CadC. As with the Cd(II) complex, the ratiometric data for the T^{5-16} peptide (Figure 4B) could be globally fit to a two-step sequential irreversible X → Y → Z reaction model (thick lines) with $k_{C7}^{app} = 6.5 \times 10^{-3}$ min^{-1} and $k_{C11}^{app} = 0.26$ min^{-1}, quite similar to the values obtained for Cd(II)-CadC. Since the fits to this model fail to fully describe the experimental data particularly at long pulse times, a second model where X is allowed to partition directly to Y or Z, that is, X → Y → Z plus X → Z (defined by k_3), was also used to fit the data (thin lines). In this case, k_2 was resolved to be 4.5×10^{-3} min^{-1}, which is similar to that of k_{C7}^{app} derived from the C^{1-10} peptide.

Reactivities of Cysteine Thiolates at Positions 7 and 11 upon Formation of Metal Complexes with Weakly Inducing Metals Zn(II) and Co(II). Zn(II) is a significant inducer of the *cad* operon in a Δ*zntA* strain of *E. coli* (*11*) but is less so in native *S. aureus*; Co(II), while a noninducing metal ion, has previously been used as spectroscopic surrogate for Zn(II) (*13*). Co(II) bound to the α3N site appears to form a highly distorted four-coordinate S_4 complex of which the spectral properties are readily bleached by the addition of stoichiometric Cd(II) and Pb(II) (*13*). Representative rPA-

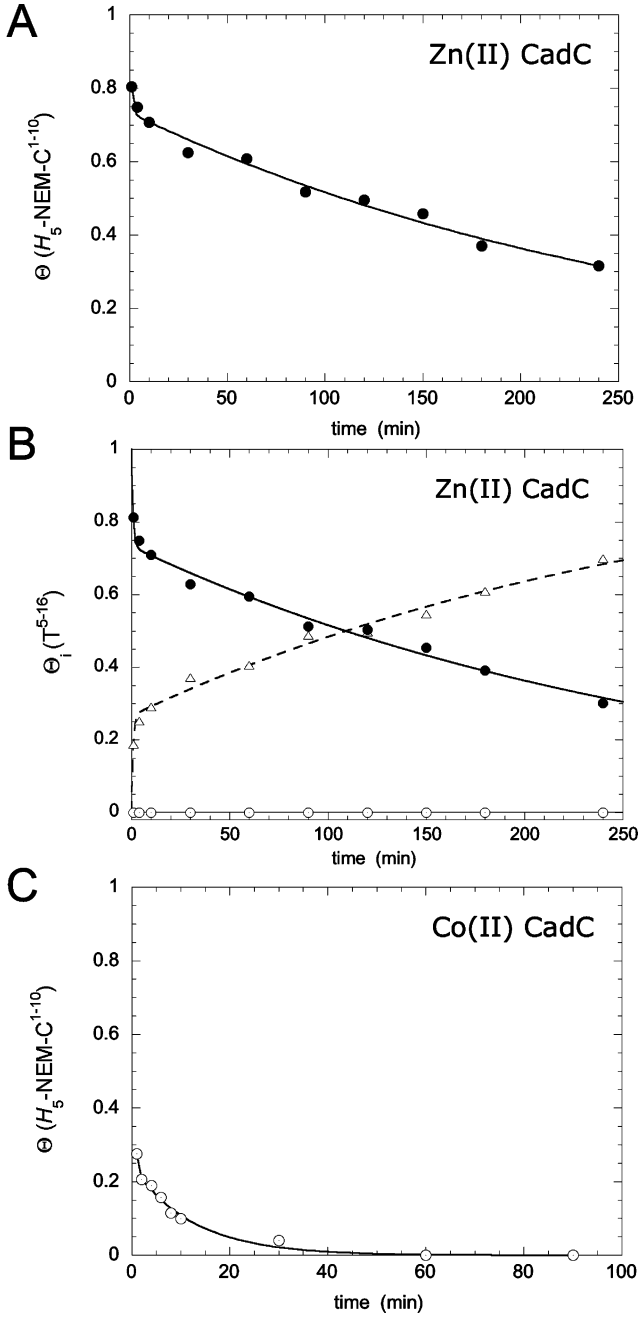

FIGURE 5: rPA-MS of $Zn(II)_2$- and $Co(II)_2$-substituted CadCs. Panel A shows the mole fraction of H_5-NEM-derivatized C^{1-10} peptide recovered from $Zn(II)_2$-CadC rPA-MS chymotryptic digests as a function of d_5-NEM pulse time. The solid line through the data is a least-squares fit to a sum of two exponentials with $k_f = 1.26 \pm 0.33$ min^{-1}, $A_f = 0.27 \pm 0.02$, $k_s = 0.0035 \pm 0.0002$ min^{-1}, and $A_s = 0.74$. Panel B shows the mole fraction of (○) H_5,H_5-, (●) d_5,H_5-, and (△) d_5,d_5-NEM-derivatized T^{5-16} peptide recovered from tryptic digests of Zn(II)-CadC as a function of d_5-NEM pulse time. Note that the disappearance of d_5,H_5-T^{5-16} (●) and the recovery of d_5,d_5-T^{5-16} (△) are described by the same rate and amplitude, $A_Y = 0.733$ and $k_2 = 0.003\,51 \pm 0.000\,20$ min^{-1}, identical to the disappearance of H_5-C^{1-10} (panel A) since derivatization of Cys11 occurs during the dead time (1 min) of the measurement. Panel C shows the mole fraction of H_5-NEM-derivatized C^{1-10} peptide recovered from $Co(II)_2$-CadC rPA-MS chymotryptic digests as a function of d_5-NEM pulse time. The solid line represents a least-squares fit to a sum of two exponentials with $k_f = 2.71 \pm 0.37$ min^{-1}, $A_f = 0.76 \pm 0.02$, $k_s = 0.080 \pm 0.0012$, and $A_s = 0.24$.

MS data are shown for $Zn(II)_2$-CadC (Figure 5A,B) compared to that of $Co(II)_2$-CadC (Figure 5C). The ratiometric

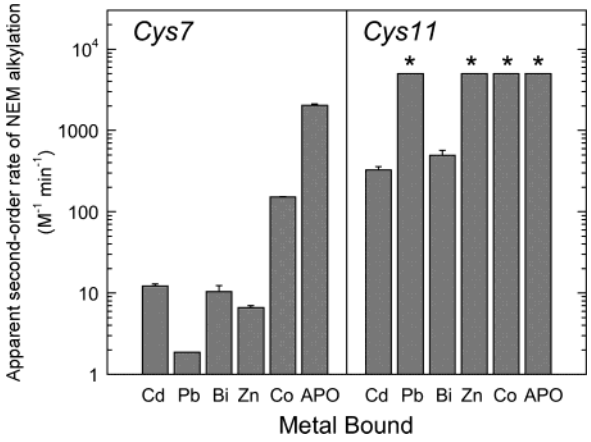

FIGURE 6: Bar chart summary of the apparent second-order rates of NEM alkylation of Cys7 (left) and Cys11 (right) in apo-CadC relative to different metal-bound complexes of CadC derived from rPA-MS progress curves such as those shown in Figures 2−5. k_{C7}^{app} for Bi(III)-CadC reflects that range (±SE) obtained from C^{1-10} and T^{5-16} peptides, the latter obtained from application of different reaction models (see text for details). For all other CadCs, k_{C7}^{app} is derived from fits obtained from C^{1-10} and T^{5-16} peptides. The ∗ denotes that only lower limits could be obtained from these thiolates, which quantitatively react within the dead time of the measurement, $k_{app} \geq 5000$ min^{-1}.

data for C^{1-10} in $Zn(II)_2$-CadC are adequately fit to a sum of two exponentials with a fractional amplitude and alkylation rate resolved for the fast-reacting thiolate of $A_f = 0.27$ and $k_f = 1.26$ min^{-1}, respectively. Assuming that this fast rate again corresponds to derivatization of Cys7 in contaminating apo-CadC, k_{C7}^{app} of $(3.5 \pm 0.2) \times 10^{-3}$ min^{-1}, or an apparent second-order rate constant of 6.6 M_{NEN}^{-1} min^{-1}, is obtained. This corresponds to a level of attenuation comparable to that of the Cd(II), Pb(II), and Bi(III) proteins. Like Pb(II)-CadC, the H_5,H_5-derivative of the T^{5-16} peptide is completely absent at earliest pulse times in $Zn(II)_2$-CadC with the rate of conversion of the H_5,d_5-T^{5-16} species to the d_5,d_5- T^{5-16} species identical to that of the conversion of H_5-C^{1-10} to d_5-C^{1-10}, that is, $k_2 = k_{C7}^{app}$ (Figure 5B). Thus, Cys11 in the $Zn(II)_2$ complex cannot be distinguished from that of apo-CadC.

Likewise, k_{C7}^{app} was found to be $(8.0 \pm 1.2) \times 10^{-2}$ min^{-1} ($A_s = 0.24$) for the $Co(II)_2$ complex for an apparent second-order rate constant of ∼150 M_{NEM}^{-1} min^{-1}, or about 30-fold faster than Zn(II)-CadC. In fact, the binding of Co(II) to the α3N site only protects Cys7 from alkylation by NEM by ∼10-fold, far less effective than the other inducing metals ions. Figure 6 summarizes the apparent second-order order rate constants of NEM alkylation of Cys7 and Cys11 in apo-CadC relative to various metalloderivatives of CadC (see Discussion).

DISCUSSION

S. aureus pI258 CadC is a metalloregulatory homodimeric repressor protein that is responsive to increased concentrations of Cd(II), Pb(II), Zn(II), and Bi(III) in the cell (*9*, *11*). The coordination structure of the regulatory metal binding site that mediates for de-repression of the *cad* operon has been extensively characterized by optical UV−vis absorption, ^{113}Cd NMR, and X-ray absorption spectroscopies of Cd(II), Pb(II), and Bi(III) complexes (*10*, *12*, *13*). These and other studies (*25*, *26*), coupled with homology modeling using the

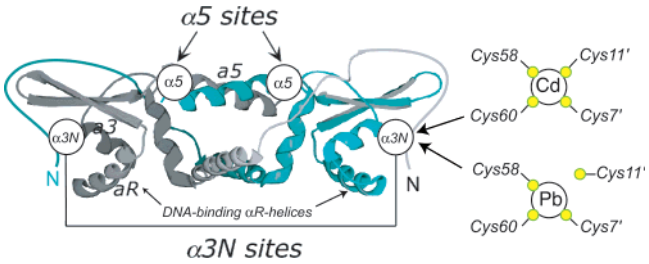

FIGURE 7: Homology model of *S. aureus* pI258 CadC using apo-SmtB as a template (*16*) indicating the general location of the α3N metal binding sites on the dimer. Cartoon models of the coordination complexes formed by Cd(II) and Pb(II) are shown on the right (*13*). Spectroscopic studies reveal that Bi(III) forms an S_4 complex exactly analogous to that formed by Cd(II) (*12*).

cyanobacterial zinc sensor SmtB as a template, are consistent with a model in which metal ions bind to two symmetry-related sites on the periphery of the dimer, denoted the α3N site. This α3N site is formed by coordination of metals to Cys7 near the N-terminus of one subunit and Cys58 and Cys60 in the putative α3 helix of the other (Figure 7) (*12*). In the Cd(II) and Bi(III) complexes, Cys11 near Cys7 in the N-terminal "arm" also donates a thiolate ligand to form an S_4 complex (Figure 7). Metal competition experiments reveal that Zn(II) and Co(II) bind to the same α3N site, but not as tightly, as well as to a second site, denoted α5 (*13*). There is as yet no high-resolution crystallographic structure of CadC; therefore, the details of the structure and reactivity of individual metal complexes is unknown. Here we use rPA-MS to probe the reactivities of two closely spaced cysteines in the N-terminal region of CadC, Cys7 and Cys11, to obtain insight into the role of individual metal−ligand coordination bonds in metal resistance in vivo.

General Considerations of the Method as Applied to CadC. To apply rPA-MS, high-resolution mass spectral identification and resolution of cysteine-containing proteolytic peptides of the underivatized and NEM-modified protein is an essential requirement. Here, we further exploit the different substrate specificities of chymotrypsin vs trypsin to obtain an independent determination of the reactivity profile of Cys7 from the C^{1-10} peptide, allowing us to unambiguously resolve the reactivity profile of Cys11 from isotopic analysis of the doubly derivatized T^{5-16} peptide.

Both Cys7 and Cys11 thiolates are highly reactive in the absence of a coordinated metal ion in apo-CadC (Figure 2A) and their reactivities are attenuated to distinct degrees when bound to different metal ions (Figure 6). Although many factors can potentially influence cysteine reactivity, for example, solvent accessibility, hydrogen bonding, and ionization state of the thiol(ate) group, it is generally accepted that metal-bound cysteines will be fully deprotonated thiolate anions, the nucleophilicity of which will be greatly attenuated upon formation of metal complexes of high thermodynamic stability (*27*) due to very slow rates of metal dissociation and perhaps even transient ligand dissociation. This is largely what is observed for Cys7. However, even in apo-CadC, there is a clear difference between the reactivities of the two thiolates. The apparent second-order rate constant for alkylation of Cys11 is at least 2-fold larger than that for Cys7 (Figure 6) and is likely much larger since only a lower limit could be obtained for k_{C11}^{app}; an upper limit is defined by glutathione, $k = 3.8 \times 10^4$ M_{NEM}^{-1} min^{-1} (*28*). Although the origin of this difference is unknown, this finding demonstrates the sensitivity of rPA/MS to uncover even small differences in free thiolate reactivity.

Although Cys7 and Cys11 are close to one another in the amino acid sequence, a significant population of H_5,d_5-derivatized T^{5-16} is consistently observed, revealing that the single-alkylated T^{5-16} species formed during the d_5-NEM pulse is a stable intermediate (Figure 1). This is clearly the case for the Pb(II), Cd(II), and $Zn(II)_2$ complexes but may underlie the complexity of the Bi(III)-CadC reaction profiles (Figure 4), which are not well described by a simple sequential model where alkylation of Cys11 is followed by Cys7. The low (~40%) recovery of H_5-NEM-C^{1-10} at early pulse time points (Figure 4) may be reporting on initial modification of cysteines other than Cys11 in Bi(III)-CadC, alkylation of which results in facile Bi(III) dissociation; this low stability of selected monoalkylated Bi(III)-chelates relative to Cd(II) and Pb(II) chelates may be influenced by the distinct net charges of the Bi(III) vs Cd(II)/Pb(II) chelates. Interestingly, functional studies suggest Cys11 plays a more pronounced role in allosteric regulation in Bi(III)-CadC than in the other metal complexes suggesting that this ligand may be more intimately incorporated into the metal complex (*12*).

It is unknown how the observed slow rate of alkylation of Cys7 is influenced by alkylation of Cys58 and Cys60 since these rates could not be measured.[2] However, the fact that the reaction profile of metal-coordinated Cys7 is well-described by a single exponential (as expected from the pseudo-first-order conditions employed here) suggests one of two possibilities: (1) the Cys7 alkylation rate is independent of alkylation of Cys58 or Cys60 thiolates, or more likely, (2) all three cysteines are alkylated at the same apparent rate. The latter scenario would occur if the remaining cysteines become highly reactive once any one of Cys7, Cys58, or Cys60 is alkylated by NEM. This would take place if metal dissociates from the bis-alkylated (Cys11 + Cys7/Cys58/Cys60) chelates. This situation occurs in HIV-1 nucleocapsid protein (*27*) and also characterizes the cysteine pair in the Cys_2−His_2 zinc finger domains of MTF-1 and Sp1, where there is no build-up of monoalkylated intermediate in any pulse time along the reaction coordinate (*19*). Consistent with a concerted alkylation of Cys7, Cys58, and Cys60, the apparent second-order alkylation rate constants for Cys7 in metallo-CadCs are essentially identical to those measured for the cysteine thiolate pairs in the N-terminal zinc finger domains of MTF-1 and Sp1 (~3.3 M_{NEM}^{-1} min^{-1}) (*19*).

rPA-MS as a Probe of Metal Coordination Number in Metallo-CadCs. Although rPA-MS obviously cannot directly determine coordination number in different metalloderivatives of CadCs, the reactivity profiles directly correlate with expectations drawn from previous spectroscopic studies of Pb(II)-, Cd(II)-, and Bi(III)-substituted CadCs. For example, X-ray (XAS) and UV−vis absorption spectroscopy of wild-type (*10*) and cysteine-substitution mutants of Pb(II)-CadC indicate that the Pb(II) ion forms a trigonal complex employing Cys7, Cys58, and Cys60 with Cys11 excluded from the first shell of ligands (Figure 7) (*13*). rPA-MS is fully compatible with these findings since the reactivity of Cys11 in the Pb(II)-complex is indistinguishable from that of apo-CadC. In contrast, it has been argued from the results of UV−vis and XAS spectra that Cd(II) is bound by four

cysteinyl ligands, Cys7, Cys11, Cys58, and Cys60 (*10*). However, ^{113}Cd NMR chemical shift of ^{113}Cd-substituted CadC revealed a single resonance at 622 ppm, more consistent with an S_3N/O or trigonal S_3 coordination geometry, rather than a typical mononuclear S_4 site (*29*, *30*). The fact that Cys11 is significantly protected from NEM alkylation in the Cd(II) complex (Figure 3) relative to the Pb(II) complex (Figure 2) suggests a structurally distorted S_4 complex rather than an S_3 complex. By the same reasoning, coordination of trivalent bismuth is most consistent with tetrathiolate coordination by rPA-MS (Figure 4); indeed, optical absorption spectra of wild-type and mutant CadCs are indicative of S_4 geometry (*12*).

The coordination geometry of Zn(II) bound to the α3N sites of CadC is unknown but may tend toward a strongly distorted S_4 complex, given the preference of Zn(II) to adopt four-coordinate vs three-coordinate complexes in proteins. However, rPA-MS reveals a reactivity profile more consistent with tris-thiolato Pb(II)-CadC vs tetrathiolate Cd(II)-CadC, since the reactivity of Cys11 is not decreased in the Zn(II) complex relative to apo-CadC (Figure 5). Since Zn(II) is smaller (ionic radius of 0.74 Å) than Cd(II) (0.92 Å), Bi(III) (1.03 Å), or Pb(II) (1.10 Å) and forms shorter metal−thiolate coordination bonds than these ions (2.3 Å vs 2.5−2.7 Å), it seems possible that Zn(II) and Co(II) (0.72 Å) are unable to simultaneously coordinate all four cysteine thiolates, which may lead to a nonoptimal or long coordination bond to, for example, Cys11. Consistent with this, the affinity of Co(II) for the α3N metal binding sites in CadC ($K_{Co}^{\alpha 3N} = 3.9 \times 10^8$ M^{-1})[2] is 4 orders of magnitude lower than that for Cd(II) (*10*). One explanation for the low recovery (~25%) of H_5-NEM-derivatized C$^{1-10}$ in the reactivity profile of Cys7 in Co(II)-CadC at early pulse time points (Figure 5C) is that once any one of the three conserved cysteines (Cys7, Cys58, or Cys60) is derivatized, Co(II) dissociates and d_5-NEM-derivatized C$^{1-10}$ quickly dominates the mixture; only when Cys11 is alkylated first can a slower rate of Cys7 (or a composite rate of Cys7, Cys58, and Cys60; vide supra) alkylation be measured. This would neatly explain the ~75% d_5-NEM-C$^{1-10}$ recovered at early pulse times. In any case, k_{C7}^{app} is still 10−50-fold larger than for the other complexes (Figure 6).

Distinct Alkylation Rates of Cys7 vs Cys11 Correlate with Distinct Functional Roles. Introduction of non-metal-liganding substitutions into the metal chelate in CadC gives rise to active CadC repressors that form stable, albeit nonnative, coordination complexes that are functionally compromised in allosteric coupling to various degrees (Figure 8) (*12*, *13*). Strikingly, glycine substitutions of Cys60 and Cys7 completely, or nearly completely, abrogate allosteric regulation of *cad* O/P binding by Pb(II) and Cd(II); interestingly, co-conservation of Cys7 and Cys60 appears to uniquely distinguish CadCs from other SmtB/ArsR metal sensor proteins (*8*). In contrast, Cys11 plays little if any functional role in coupling metal-site binding to allosteric regulation of *cad* O/P binding despite forming coordination bonds to Cd(II) and Bi(III). Therefore a correlation exists between functional importance at the level of regulation of DNA binding and intrinsic reactivity. The critical allosteric ligand Cys7 is significantly protected from alkylation, compatible with a strong coordination bond to the metal that dampens

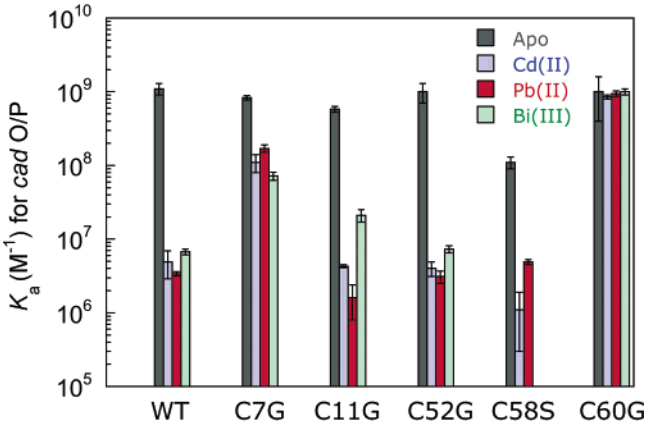

FIGURE 8: Bar chart representation of the binding affinities of wild-type and mutant CadCs for a 34-bp DNA oligonucleotide harboring a single *cad* O/P 12-2-12 inverted repeat (K_a) in the absence (apo) and presence of stoichiometric Cd(II), Pb(II), or Bi(III). This plot summarizes work previously published (*8*, *10*, *12*, *13*).

even transient dissociation of the thiolate ligand from the metal ion. This attenuation in reactivity is most pronounced in the Pb(II) derivative; this likely reflects the distinct structures of the trigonal S_3 Pb(II) complex relative to the distorted four-coordinate Cd(II) and Bi(III) complexes. In contrast, Cys11, while donating a first shell ligand to both Cd(II) and Bi(III) and perhaps Co(II), is far more reactive than Cys7 in apo-CadC and provides less protection to derivatization in all metalloderivatives.

These data suggest that Cys11 defines a weak point in these metalloregulatory complexes and is therefore a good candidate for engaging in favorable ligand exchange reactions with metal acceptor proteins, similar to that originally envisioned by copper-specific metallochaperones (*31*). This would allow the toxic metal ion to efficiently migrate from CadC sensor sites via metal ligand exchange to the actual sites of metal resistance, for example, the metal efflux pump, CadA (*2*), and perhaps other acceptor molecules. Interestingly, recent findings with another SmtB/ArsR cadmium/lead sensor, *Mycobacterium tuberculosis* CmtR, are also consistent with the presence of three, rather than four, strong thiolate ligands that play critical *functional* roles in Cd/Pb sensing in vivo, despite the fact that a fourth potentially liganding cysteine residue is nearby in the deduced homology model of CmtR (*32*). Although the metal coordination numbers, geometry, and ligand reactivity profiles of metal-coordinated cysteines in CmtR are unknown (*32*), the concept of an entry site for ligand exchange, accomplished either with a low coordination number or a weakly coordinated ligand in a coordinately saturated metal chelate, may be a general characteristic of metalloregulatory sites that function in metal resistance (cf. refs *4* and *33*). In the related zinc sensors, cyanobacterial SmtB (*14*, *34*) and *S. aureus* CzrA (*35*), the carboxyl-terminal ligand in the α5 sites (*36*) may perform this role.[3]

Such a ligand exchange reaction would seem to be a virtual requirement for effectively facilitating the movement of metal

[3] Substitution of α5 site zinc ligand Glu120 and Cys121 in *Synechococcus* SmtB (*34*) has little effect on negative regulation of operator/promoter binding in vitro (X. Chen, M. VanZile, and D. Giedroc, unpublished observations).

[4] L. Busenlehner and D. Giedroc, unpublished observations.

ions bound to regulatory sites to potential acceptor sites provided by membrane-bound efflux pumps or intracellular chelators, since the high thermodynamic stability of these complexes ($K_{Me} \geq 10^{12}$ M^{-1}) (*8*, *33*, *34*, *37*) predicts an extremely slow rate of metal dissociation into bulk solution. This is now known to be the case for Pb(II)-CadC, with $k_{off} \leq 10^{-5}$ s^{-1}.[4] This is analogous to the proposed roles of the thiolate ligands in Cu complexes formed by copper chaperones in the delivery of Cu to specific enzyme acceptor sites (*15*, *31*, *38*). Application of rPA-MS to examine the intrinsic reactivities or nucleophilicities of individual cysteine residues in Atx1 (*38*) and Atx1-like (*39*) domains may represent a productive line of investigation for understanding the mechanism of metal transfer in these systems (*15*, *40*). These experiments are currently in progress for other SmtB/ArsR metal sensor−metal acceptor pairs associated with metal resistance in prokaryotes.

ACKNOWLEDGMENT

The authors thank Dr. Bill Russell, Laboratory for Biological Mass Spectrometry at Texas A&M University, for his help in acquiring some of the MALDI-TOF spectra and Dr. Thomas O. Baldwin, University of Arizona, for his continued interest in this project.

REFERENCES

1. Rosen, B. P. (1996) Bacterial resistance to heavy metals and metalloids, *J. Biol. Inorg. Chem. 1*, 273−277.
2. Rosen, B. P. (2002) Transport and detoxification systems for transition metals, heavy metals and metalloids in eukaryotic and prokaryotic microbes. *Comp. Biochem. Physiol., Part A: Mol. Integr. Physiol. 133*, 689−693.
3. Nies, D. H., and Brown, N. L. (1998) in *Metal Ions in Gene Regulation* (Silver, S., and Walden, W., Eds.) pp 77−103, Chapman & Hall, New York.
4. Finney, L. A., and O'Halloran, T. V. (2003) Transition metal speciation in the cell: insights from the chemistry of metal ion receptors. *Science 300*, 931−936.
5. Turner, J. S., Glands, P. D., Samson, A. C. R., and Robinson, N. J. (1996) Zn^{2+}-sensing by the cyanobacterial metallothionein repressor SmtB: different motifs mediate metal-induced protein-DNA dissociation, *Nucleic Acids Res. 19*, 3714−3721.
6. Endo, G., and Silver, S. (1995) CadC, the transcriptional regulatory protein of the cadmium resistance system of *Staphylococcus aureus* plasmid pI258, *J. Bacteriol. 177*, 4437−4441.
7. Shi, W., Wu, J., and Rosen, B. P. (1994) Identification of a putative metal binding site in a new family of metalloregulatory proteins, *J. Biol. Chem. 269*, 19826−19829.
8. Busenlehner, L. S., Pennella, M. A., and Giedroc, D. P. (2003) The SmtB/ArsR family of metalloregulatory transcriptional repressors: Structural insights into prokaryotic metal resistance, *FEMS Microbiol. Rev. 27*, 131−144.
9. Yoon, K. P., Misra, T. K., and Silver, S. (1991) Regulation of the cadA cadmium resistance determinant of *Staphylococcus aureus* plasmid pI258, *J. Bacteriol. 173*, 7643−7649.
10. Busenlehner, L. S., Cosper, N. J., Scott, R. A., Rosen, B. P., Wong, M. D., and Giedroc, D. P. (2001) Spectroscopic properties of the metalloregulatory Cd(II) and Pb(II) sites of *S. aureus* pI258 CadC, *Biochemistry 40*, 4426−4436.
11. Rensing, C., Sun, Y., Mitra, B., and Rosen, B. P. (1998) Pb(II)-translocating P-type ATPases, *J. Biol. Chem. 273*, 32614−32617.
12. Busenlehner, L. S., Apuy, J. L., and Giedroc, D. P. (2002) Characterization of a metalloregulatory bismuth(III) site in *Staphylococcus aureus* pI258 CadC repressor, *J. Biol. Inorg. Chem. 7*, 551−559.
13. Busenlehner, L. S., Weng, T. C., Penner-Hahn, J. E., and Giedroc, D. P. (2002) Elucidation of primary (α3N) and vestigial (α5) heavy metal- binding sites in *Staphylococcus aureus* pI258 CadC: Evolutionary implications for metal ion selectivity of ArsR/SmtB metal sensor proteins, *J. Mol. Biol. 319*, 685−701.
14. VanZile, M. L., Chen, X., and Giedroc, D. P. (2002) Allosteric negative regulation of *smt* O/P binding of the zinc sensor, SmtB, by metal ions: a coupled equilibrium analysis, *Biochemistry 41*, 9776−9786.
15. Banci, L., Bertini, I., Ciofi-Baffoni, S., Del Conte, R., and Gonnelli, L. (2003) Understanding copper trafficking in bacteria: Interaction between the copper transport protein CopZ and the N-terminal domain of the copper ATPase CopA from *Bacillus subtilis*, *Biochemistry 42*, 1939−1949.
16. Cook, W. J., Kar, S. R., Taylor, K. B., and Hall, L. M. (1998) Crystal structure of the cyanobacterial metallothionein repressor SmtB: A model for metalloregulatory proteins, *J. Mol. Biol. 275*, 337−346.
17. Sun, Y., Wong, M. D., and Rosen, B. P. (2001) Role of cysteinyl residues in sensing Pb(II), Cd(II), and Zn(II) by the Plasmid pI258 CadC Repressor, *J. Biol. Chem. 276*, 14955−14960.
18. Apuy, J. L., Park, Z.-Y., Swartz, P. D., Dangott, L. J., Russell, D. H., and Baldwin, T. O. (2001) Pulsed-alkylation mass spectrometry for the study of protein folding and dynamics: Application to the study of the folding and assembly of bacterial luciferase, *Biochemistry 40*, 15155−15163.
19. Apuy, J. L., Chen, X., Russell, D. R., Baldwin, T. O., and Giedroc, D. P. (2001) Ratiometric pulsed alkylation-mass spectrometry of the cysteine pairs in individual zinc fingers of MRE-binding transcription factor-1 (MTF-1) as a probe of zinc chelate stability, *Biochemistry 40*, 15164−15175.
20. Silverman, J. A., and Harbury, P. B. (2002) Rapid mapping of protein structure, interactions, and ligand binding by misincorporation proton-alkyl exchange, *J. Biol. Chem. 277*, 30968−30975.
21. Wang, S., Zhang, X., and Regnier, F. E. (2002) Quantitative proteomics strategy involving the selection of peptides containing both cysteine and histidine from tryptic digests of cell lysates, *J. Chromatogr. A 949*, 153−162.
22. Sebastiano, R., Citterio, A., Lapadula, M., and Righetti, P. G. (2003) A new deuterated alkylating agent for quantitative proteomics, *Rapid Commun. Mass Spectrom. 17*, 2380−2386.
23. Pasquarello, C., Sanchez, J. C., Hochstrasser, D. F., and Corthals, G. L. (2004) N-*t*-butyliodoacetamide and iodoacetanilide: two new cysteine alkylating reagents for relative quantitation of proteins, *Rapid Commun. Mass Spectrom. 18*, 117−127.
24. Nicoli, M. Z., and Hastings, J. W. (1974) Bacterial luciferase. The hydrophobic environment of the reactive sulfhydryl, *J. Biol. Chem. 249*, 2393−2396.
25. Sun, Y., Wong, M. D., and Rosen, B. P. (2002) Both metal binding sites in the homodimer are required for metalloregulation by the CadC repressor, *Mol. Microbiol. 44*, 1323−1329.
26. Wong, M. D., Lin, Y. F., and Rosen, B. P. (2002) The soft metal ion binding sites in the *Staphylococcus aureus* pI258 CadC Cd-(II)/Pb(II)/Zn(II)-responsive repressor are formed between subunits of the homodimer, *J. Biol. Chem. 277*, 40930−40936.
27. Chertova, E. N., Kane, B. P., McGrath, C., Johnson, D. G., Sowder, R. C., II, Arthur, L. O., and Henderson, L. E. (1998) Probing the topography of HIV-1 nucleocapsid protein with the alkylating agent *N*-ethylmaleimide, *Biochemistry 37*, 17890−17897.
28. Lundblad, R. J. (1991) The modification of cysteine, *Chemical Reagents for Protein Modification*, 2nd ed., pp 59−103, CRC Press, Boca Raton, FL.
29. Matzapetakis, M., Farrer, B. T., Weng, T. C., Hemmingsen, L., Penner-Hahn, J. E., and Pecoraro, V. L. (2002) Comparison of the binding of cadmium(II), mercury(II), and arsenic(III) to the de novo designed peptides TRI L12C and TRI L16C, *J. Am. Chem. Soc. 124*, 8042−8054.
30. Summers, M. F. (1988) ^{113}Cd NMR spectroscopy of coordination compounds and proteins, *Coord. Chem. Rev. 86*, 43−134.
31. Rae, T. D., Schmidt, P. J., Pufahl, R. A., Culotta, V. C., and O'Halloran, T. V. (1999) Undetectable intracellular free copper: the requirement of a copper chaperone for superoxide dismutase, *Science 284*, 805−808.
32. Cavet, J. S., Graham, A. I., Meng, W., and Robinson, N. J. (2003) A cadmium-lead-sensing ArsR-SmtB repressor with novel sensory sites. Complementary metal discrimination by NmtR and CmtR in a common cytosol, *J. Biol. Chem. 278*, 44560−44566.
33. Banci, L., Bertini, I., Ciofi-Baffoni, S., Finney, L. A., Outten, C. E., and O'Halloran, T. V. (2002) A new zinc-protein coordination site in intracellular metal trafficking: solution structure of the apo and Zn(II) forms of ZntA(46−118), *J. Mol. Biol. 323*, 883−897.
34. VanZile, M. L., Chen, X., and Giedroc, D. P. (2002) Structural characterization of distinct α3N and α5 metal sites in the cyanobacterial zinc sensor SmtB, *Biochemistry 41*, 9765−9775.

35. Pennella, M. A., Shokes, J. E., Cosper, N. J., Scott, R. A., and Giedroc, D. P. (2003) Structural elements of metal selectivity in metal sensor proteins, *Proc. Natl. Acad. Sci. U.S.A. 100*, 3713−3718.
36. Eicken, C., Pennella, M. A., Chen, X., Koshlap, K. M., VanZile, M. L., Sacchettini, J. C., and Giedroc, D. P. (2003) A metal-ligand-mediated intersubunit allosteric switch in related SmtB/ArsR zinc sensor proteins, *J. Mol. Biol. 333*, 683−695.
37. Outten, C. E., and O'Halloran, T. V. (2001) Femtomolar sensitivity of metalloregulatory proteins controlling zinc homeostasis, *Science 292*, 2488−2492.
38. Pufahl, R. A., Singer, C. P., Peariso, K. L., Lin, S.-J., Schmidt, P. J., Fahrni, C. J., Culotta, V. C., Penner-Hahn, J. E., and O'Halloran, T. V. (1997) Metal ion chaperone function of the soluble Cu(I) receptor Atx1, *Science 278*, 853−856.
39. Wernimont, A. K., Huffman, D. L., Lamb, A. L., O'Halloran, T. V., and Rosenzweig, A. C. (2000) Structural basis for copper transfer by the metallochaperone for the Menkes/Wilson disease proteins, *Nat. Struct. Biol. 7*, 766−771.
40. Arnesano, F., Banci, L., Bertini, I., Cantini, F., Ciofi-Baffoni, S., Huffman, D. L., and O'Halloran, T. V. (2001) Characterization of the binding interface between the copper chaperone Atx1 and the first cytosolic domain of Ccc2 ATPase, *J. Biol. Chem. 276*, 41365−41376.
41. Barbacci, D. C., Edmondson, D. H., and Russell, D. H. (1997) Evaluation of the variables that affect resolution in the delayed extraction MALDI-TOF, *Int. J. Mass Spectrom. Ion Processes 165−166*, 221−235.

BI035668F